26th ABCM International Congress of Mechanical Engineering
November 22-26, 2021. Florianópolis, SC, Brazil

COB-2021-0957
ANALYSIS OF PARTICLES SEDIMENTATION IN SHEAR-THINNING FLUID: SETTLING VELOCITY, DRAG COEFFICIENT, AND SETTLING TRAJECTORIES COMPARISON

Victor Emanuel Santana[a]
Yamid J. García-Blanco[a]
Eduardo Matos Germer[a]
Admilson T. Franco[a]

[a] Federal University of Technology- Paraná- UTFPR, Research Center for Rheology and Non-Newtonian Fluids – CERNN, 81280-340, Rua Deputado Heitor Alencar Furtado 5000 – Ecoville, Curitiba_PR, Brazil
victors.1999@alunos.utfpr.edu.br, yamidblanco@alunos.utfpr.edu.br, eduardomg@utfpr.edu.br, admilson@utfpr.edu.br

Abstract. *In recent years, the Oil and Gas industry has focused on predicting and controlling the different processes involved in oil and gas production, such as the control and prediction of cutting sedimentation during the drilling process. The importance of the subject is to understand the fluid-solid interactions during sedimentation in non-Newtonian fluids. The present work has as objective the contribution to understand and describe the cuttings sedimentation process during the well drilling operation and provide reliable data for future validations of numerical studies related to the sedimentation phenomenon. Therefore, an Arduino infrared release system was developed to settle one particle at the center of a rectangular tank filled by a working fluid in standardized conditions. The first stage of the study was the validation of the experimental setup, whereby tests were performed releasing spherical and non-spherical particles in Newtonian fluids. The results of the settling velocity and drag coefficient were compared with analytical correlations available in the literature. Later, tests with spheres were performed in a fluid with shear-thinning rheological characteristics. The Power-law model well represents such rheological characteristics. The settling velocity and the drag coefficient were also obtained, followed by the particles during the sedimentation process. The drag coefficient showed higher values for non-Newtonian fluid than the Newtonian case, contrary to the behavior of the settling velocity, which tends to be higher for the sedimentation in the Newtonian fluid. The particle's sedimentation path shows straight and oblique behaviors for the non-Newtonian fluid. For the case of Newtonian fluids, a straight behavior was presented for Reynolds between 50 and 200, for Reynolds close to 300 an oblique behavior was depicted, for Reynolds around to 450 an oblique intermittent behavior and the cases for high Reynolds numbers, between 2000 and 9000, straight and oblique sedimentation trajectories are observed. As proposed, was analyzed the influence of rheological proprieties and conclude that seems affected the sedimentation regime of the particles, the particle shape is another factor of influence, the not spherical particle tends to have more disturbed sedimentation than a sphere.*

Keywords: *Shear-thinning fluid, spherical particles, non-spherical particles, sedimentation*

1. INTRODUCTION

The sedimentation of particles can be described as the free fall of a particle into a fluid. It is a seemingly simple problem but involves complex and intriguing physics. The sedimentation of particles has great importance in engineering and nature sciences since this phenomenon can be observed in many industrial processes, such as drilling on oil wells, in homogenization processes in the food industry, in grain transportation, as well as in some natural phenomena, such as lava flow, pollutant sedimentation, plant pollination, among others. Therefore, most of the studies in this area have as objective identify sedimentation patterns and use them for particle trajectories prediction.

During the particle sedimentation in a homogeneous fluid, the particle is submitted to various forces, the main of which are the weight, F_W, the drag force, F_D, and the buoyancy force, F_B (Elgaddafi et al., 2012). According to Nunes et al. (2004) when a sphere with diameter, d, and density, ρ_s, sediments in a viscous fluid, with density ρ_f, where the friction between fluid and particle have considerable importance in resistance force to the movement, and considering the media as infinity despising the wall effects, under the gravitational effect, g, the particle accelerates until the balance between the weight force, F_W, the drag force, F_D, and the buoyancy force, F_B, is reached, as shown in Figure 1. In this stage, the particle reaches a maximum constant velocity, known as settling velocity, v_t.

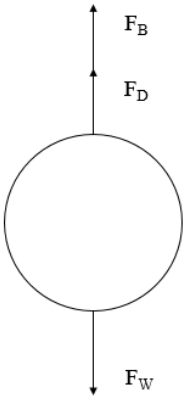

Figure 1. Forces acting during particle sedimentation.

Eltilib et al. (2011) stated that the sedimentation behavior depends on particle shape and density. In this way, the settling velocity of a spherical particle will be different from an irregular shape particle. The work proposed by Song et al. (2017) is an example of an experimental study in this area. This study formulates a new model for the drag coefficient in Newtonian fluids for spheres and particles with non-spherical shapes (cubic and cylindrical).

The objective of the present study is to understand the cuttings sedimentation during the drilling process of oil wells, where different variables are involved, such as the particle-particle and the wall-particle interactions, the rheological characteristics of the fluid, the effect of particle constitution, and the impact of fluid's shear history. Therefore, to better analyze this phenomenon and consequently reduce eventual losses in the drilling process still necessary experimental and numerical studies, which aim to understand the effects of these variables in isolation, and later the understanding of the whole phenomenon. Shear-thinning properties characterize the drilling fluids used in the drilling activities, the viscosity of such fluids decreases with the increase of the deformation over the fluid. After cessation of the imposed deformation, its viscosity returns to a high value.

The settling velocity is essential since its terminal value and the time to reach this critical velocity allow determining the number of cuttings that will sediment until the fluid gains enough consistency to stop the sedimentation process. It is also important to estimate the time that the process can be stopped before the formed bed becomes too big to make difficult or impossible the restart of drilling. For these reasons, it is interesting for the oil industry to further understand and predict how the sedimentation process occurs and consequently evaluate these effects in normal occurrences during the drilling process—for example, predicting the height of the bed of cuttings that can be formed when the drilling process is stopped or during the interruption of the drilling fluid circulation.

Reynolds and Jones (1989) published an interesting experimental study of settling velocities of particles in non-Newtonian fluids. To validate the experimental bench, they made tests with Newtonian fluids and compared the settling velocities obtained experimentally with the settling velocities calculated with equations proposed by Kao and Hwang (1980), Concha and Almendra (1979), and Brauer and Sucker (1976) to plot a master curve of particle settling in a Power-law fluid.

Horowitz and Williamson (2010) carried out an experimental study of the influence of the Reynolds number (on a track from 100 to 1500) in the free fall dynamics and ascension of spherical particles in fluids. There were 133 combinations of Re and mass ratio ($m^* = \rho_s/\rho_f$). In this work, a regime map of the trajectories was generated for the different particles. A transition from steady vertical to chaotic paths and high-frequency oscillatory behavior are depicted.

Also, Veldhuis and Biesheuvel (2007) presented an investigation experiment of the movement regime of spheres in free fall and ascent. They divide the results into seven different cases, showing the regimes obtained for each Galileo number and particle tested. In this study, they verify the conclusions presented by Jenny et al. (2003) for this phenomenon and conclude that the results of the studies have good agreement.

Xu et al. (2018) presented an interesting study about the settling behavior of non-spherical particles in Power-law fluids. They made 553 tests varying Reynolds, sphericity, and shear-thinning index to propose a correlation for drag coefficient and settling velocity as a function of the particle and fluid properties. Different types of particle shapes were used in this study: spherical, cubic and cylindrical, and eight different particle sphericities, then it is possible to use this correlation for particles with irregular shapes, which makes the correlation very interesting for analyzing the behavior of cuttings in a drilling process.

Therefore, due to the scarcity of experimental sedimentation data in non-Newtonian fluids, an experimental study is carried out to generate reliable data of settling velocity, drag coefficient and sedimentation trajectory for different particles in different fluid media: Newtonian fluids and non-Newtonian fluids with prominent shear-thinning characteristics. Also, the present experimental study is addressed to the understanding and description of cuttings sedimentation during the well-drilling processes and to provide data for future validations of numerical studies related to this phenomenon.

2. METODOLOGY

2.1 Experimental apparatus

For the present study was built an acrylic tank with a square section of 0.2 × 0.2 m and 1.2 m height. It was installed a stainless-steel ball valve ¾" and a semicircular shell was connected at the bottom of the tank to ensure easy removal of the settled particles. A plate with a circular hole was positioned at the top of the 1 m from the tank bottom to guarantee the particle releasing in the tank's centerline. The tank walls were attached to the base using screws and sealing rings, while the connection between the walls was reinforced with acrylic glue. Figure 2 presents a schematic diagram of the tank.

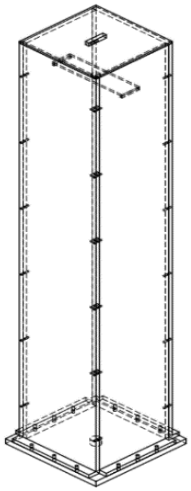

Figure 2. Schematic diagram of the settling tank.

Figure 3 shows the releasing system developed for settling one particle at a time at the center of the tank. It works through a claw controlled by an Arduino system with an infrared (IR) board, remote control, and servo motor.

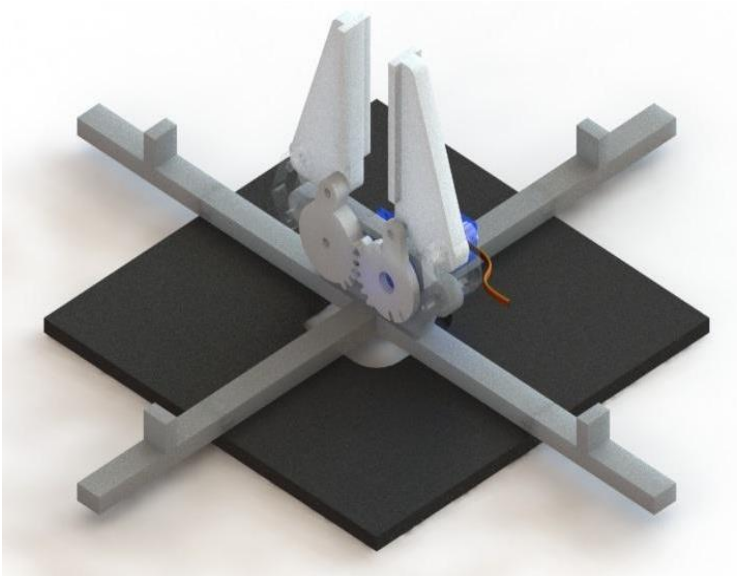

Figure 3. 3D design of the claw system.

2.2 Particles

Three types of particles were used for tests, Delrin and tungsten spheres, as also ellipsoids printed in resin material. Table 1 summarizes the different material properties and the sphere diameters used in the current study.

Table 1. Properties and material of the different spheres used in the present study.

Diameter [mm]	Material	Density (ρ)
3.175 4.75 6.35 8 10	Delrin® - Polyacetal	1410 kg/m^3
2 3 4.76 5.56	Tungsten	14800 kg/m^3

For the case of non-spherical particles, an ellipsoid configuration was used. The geometrical configuration is vital for the further analysis of the settling data. Figure 4 indicates the different geometrical aspects used for non-spherical particles. The letters a, b, and c indicate the principal axis for the ellipsoidal configuration, where the flatness for ellipsoidal particles is defined by the c/a ratio. These ellipsoids were printed on 3DFila resin that provided a better surface quality.

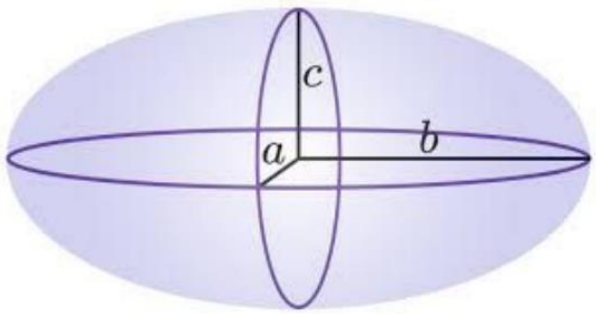

Figure 4. Illustration of the ellipsoid and the dimensions used to identify them in Table 2.

Table 2. Geometrical aspect and properties of the ellipsoid particles.

Flatness	a [mm]	b [mm]	c [mm]	Material	Density (ρ)
1/2	4	4	2	Resin	1161 kg/m^3
2	2	2	4		
1/3	4.5	4.5	1.5		
3	1.5	1.5	4.5		

2.3 Working fluids

For the present study, different fluids were used: water and a water-glycerin mixture in the proportion of 50 wt% were used as Newtonian fluids. A Carbopol® 940 0.08 wt% solution with water was used as shear-thinning fluid with behavior well described by the Power-law model. During the rheology tests of the Carbopol® 0.08 wt% solution, the shear stress value was close to the order of magnitude of the minimum torque of the rheometer, and due to the standard deviation of this value, the yield stress value is negligible. Figure 5 depicts the flow curves obtained for the different fluids. For a better understanding, the fluids will be named N1, N2, C1, for water, water-glycerine 50 wt% and Carbopol® 0.08wt% solution, respectively.

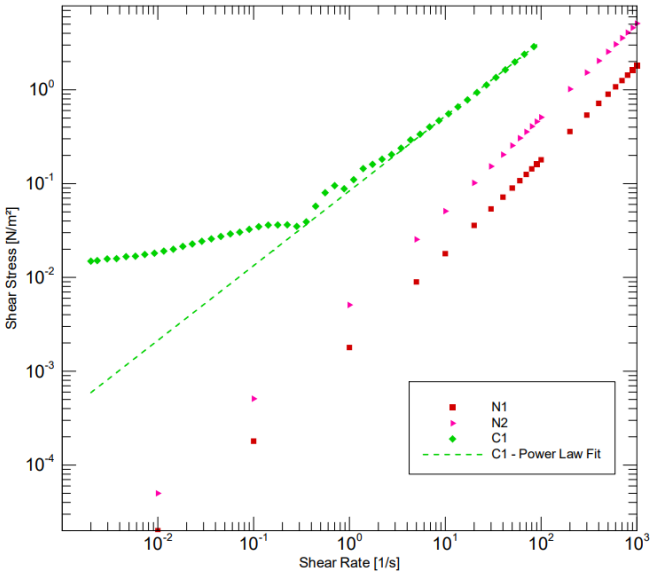

Figure 5. Dynamic flow curves for the different working fluids.
Solid-lines represent a model fitting for each fluid.

Table 3 summarized the rheological parameter fit by the different rheological models.

Table 3. Fluid properties of the different working solutions

Fluid	**Composition**	**Density**	**Viscosity**	**Shear-thinning index**	**Yield stress**	**Consistency coefficient**
		ρ [kg/m³]	**μ [m²/s]**	**n**	**τ**	**K**
N1	Water	998	0,001792	-	-	-
N2	Glycerin 50 wt %	1150	0,005086	-	-	-
C1	Carbopol® 0.08 wt%	1022	-	0.7046	-	0.0843

2.4 Experimental procedure

The experimental methodology was divided into two parts: a preliminary setup stage and the execution of the experiment. Preliminary setup stage was started by pouring the fluid into the tank that is sufficient to pass the guide (so that the spheres are released from inside the fluid). After filling the tank, it is necessary to let it rest for at least 12 hours to guarantee that there are not bubbles that hinder the visualization of the experiment. Then, a thermocouple was placed in the fluid until the stabilization of the fluid temperature to 20 °C. A camera was placed one meter away from the front of the tank and at half of the tank height to ensure a good visualization field. Also, the lighting was adjusted with the reflector to avoid shadows at the bottom of the tank.

For the experiment, one must take the particles with the claw, position the claw above the tank, start recording, release the ball, once the particle reaches the tank bottom, the ball is removed. The procedure is repeated three times with the same particle, in the same way, the procedure is repeated with the other configurations for a better statistical representation of the phenomena. In Figure 6, it is possible to observe the particle release system positioned on the tank top and the sphere being released after the activation of the IR system by the remote control.

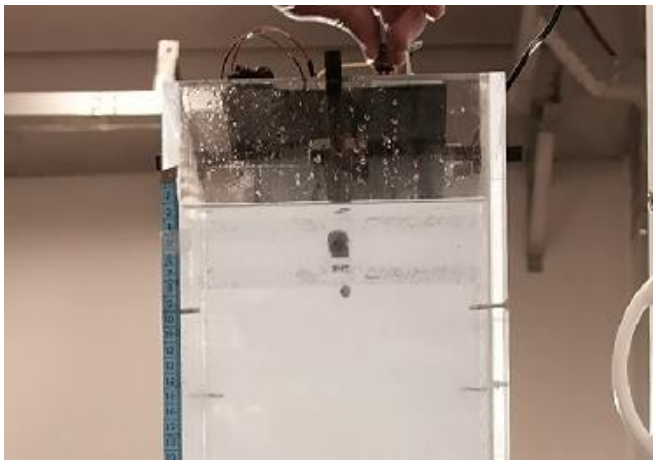

Figure 6. Particle release in the experiment.

2.5 Collecting and processing data

The data obtained from the experimental tests were recorded through video, the position of the sphere concerning time was analyzed using a tape measure glued to the front of the tank. Besides, the Tracker software was used for particle tracking and speed calculation. Tracker is a free video analysis software that provides the particle's position in each instant of time by analyzing the recording frames. With the data obtained, the software also plots graphs and assembles position tables on the horizontal and vertical axes, the speeds on the axes, the scalar speed and particle acceleration. The video can define a real size reference on a scale by creating a virtual ruler from the measuring tape fixed inside the tank.

Figure 7 shows the x and y axes adjusted according to the camera's position in each recording. The red lines in Fig. 7 show the sphere's location in different video frames, also are presented the plotted graphs and assembled tables are also presented.

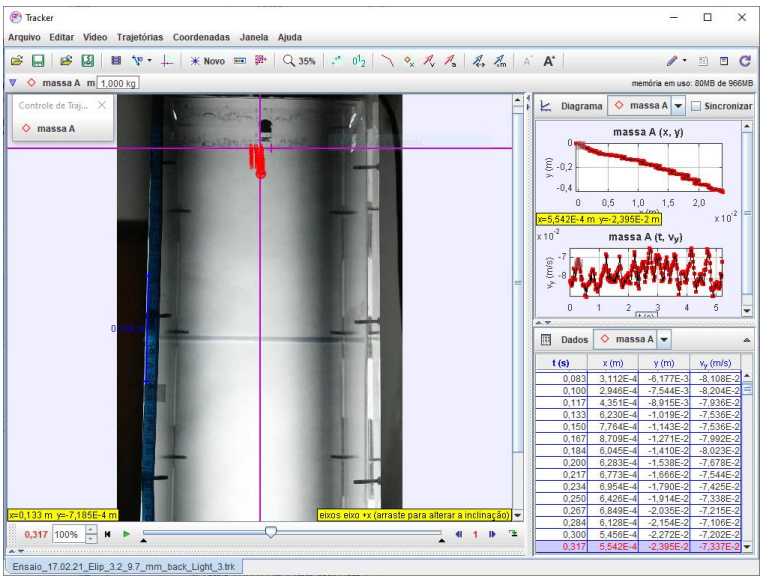

Figure 7. Treatment of data on Tracker.

2.6 Parallax error

The parallax error can be defined as a measurement error related to distance when a measurement depends on the field of view, such as an image or video system. In this experiment, the influence of this error is verified using three videos made from different positions: one above, one in the middle, and one below, so that it was possible to compare a terminal speed obtained in each of the videos and to compare the variation of the selected values with the specifics without this analysis of the perspective. The videos were made with a 10 mm diameter sphere due to the ease of visualization of this partition. A low standard deviation was obtained from the parallax test, a maximal value of 0.0021 m/s was reached

for the terminal velocity from the three videos. Therefore, for the present experimental study, the parallax error was neglected.

3. RESULTS

In Table 4, the Reynolds number equations are used to parameterize the different fluids used in this work, for non-spherical particles was defined an equivalent diameter, de, where this diameter represents a sphere with an equivalent volume of non-spherical particles. For the Power-law fluid was used the generalized Reynolds number.

Table 4. Reynolds number used with different fluids and particles.

Reynolds Equations	
Non-Spherical particle in Newtonian fluid	$Re = \frac{\rho_f V_t d_e}{\mu}$
Non-Spherical particle in Power-law fluid	$Re = \frac{\rho_f {V_t}^{2-n} {d_e}^n}{K}$
Spherical particle in Power-law fluid	$Re = \frac{\rho_f {V_t}^{2-n} d^n}{K}$

3.1 Spheres

Figure 8 shows the results obtained in the tests for the different spherical particles. In Figure 8a, the average velocities by the dimensionless diameter are presented. Dimensionless diameter is the ratio between the diameter of the particle, or equivalent diameter, and the width of the tank. Figure 8b shows the drag coefficient as a function of the dimensionless diameter of the spheres. Figure 8c is the Reynolds number by the dimensionless diameter of the terminal velocities. In fluid N1, the material of the spheres used was tungsten, the Reynolds range is 2000 to 9000, for fluid N2, the material of the spheres used was polyacetal, and the Reynolds number range is between 50 and 450, for fluid C1, the material of the spheres used was polyacetal, and the Reynolds range is 20 to 60.

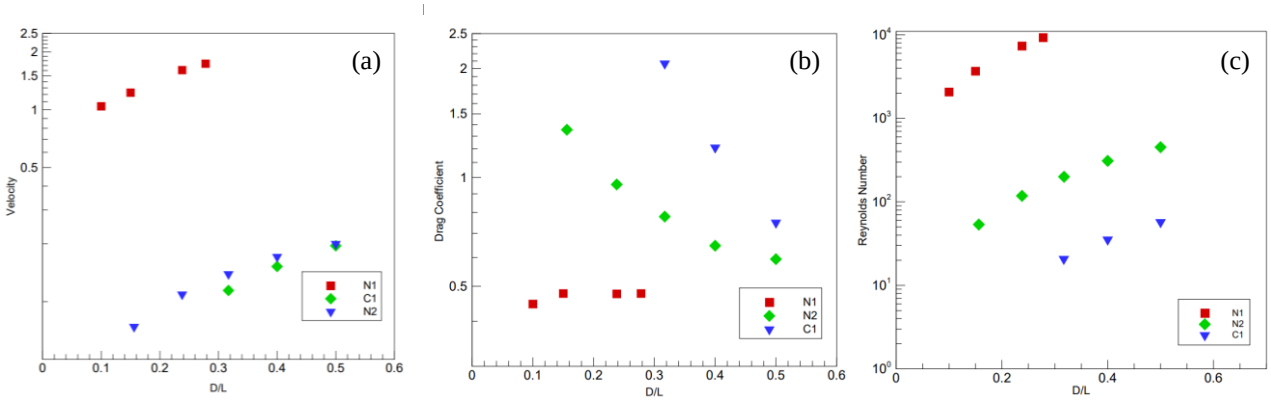

Figure 8. Experimental results presented as a relationship with the dimensionless diameter. a) Average terminal velocity by the dimensionless diameter. b) Average C_D by the dimensionless diameter. c) Average Reynolds by the dimensionless diameter.

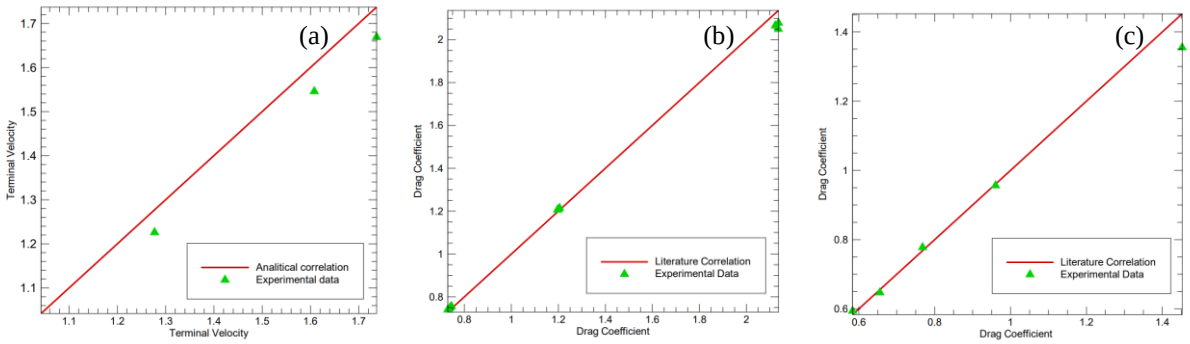

Figure 9. Experimental results presented in comparison the correlations founded in literature.
a) Terminal velocity for N1 fluid. b) Drag coefficient for N2 Fluid. c) Drag coefficient for C1 fluid.

In Figure 9 are presented the analytical values from correlations found in the literature. For fluid N1 were used the equation proposed by Zanker (1980), for fluid N2 the data correlation for drag coefficient for sphere proposed by Morrison (2013) because the Zanker equation was not applicable for this Reynolds range. For fluid C1 were used the equation for drag coefficient generalized for Power-law fluids proposed by Renauld et al. (2004), which was developed for spheres settling in Power-law fluids. It is possible to observe there is a significant agreement between them, which the maximum value for error is 6.7%.

Table 5. Drag coefficient and terminal velocity equations for settling for spheres.

Models	**Equations**
Zanker (1980)	$V_t = 1.74\left[dg\left(\frac{\rho_p}{\rho_f}-1\right)\right]^{1/2}$
Morrison (2013)	$C_D = \frac{24}{Re} + \frac{2.6\left(\frac{Re}{5.0}\right)}{1+\left(\frac{Re}{5.0}\right)^{1.52}} + \frac{0.411\left(\frac{Re}{5.0}\right)^{-7.94}}{1+\left(\frac{Re}{263000}\right)^{-8.00}} + \left(\frac{Re^{0.80}}{461000}\right)$
Renauld *et al.* (2004)	$C_D = C_{Do} + \frac{A_c}{A_m} C_{Do} {C_{Do}}^{2\beta} \left(\frac{6X(n)}{6X(n)b + C_{Do}}\right)^{\beta} + C_{D\infty}\left(\frac{6X(n)b}{6X(n)b + 128C_{Do}}\right)^{\frac{11}{12}}$
Balance of forces	$C_D = \frac{4}{3}\frac{dg}{{V_t}^2}\left(\frac{\rho_p - \rho_f}{\rho_f}\right)$

Table 5 summarizes the correlations used to compare the experimental data obtained. The equation developed by Zanker uses Newton's theory for a fluid (fluid consisting of discrete particles), and has a validity range of Reynolds of Re > 700-1000. Morrison's equations were developed to correlate the entire range of Reynolds numbers, from creeping flow until reaching the highest values of Reynolds numbers in turbulent flows. Thus, the proposed relationship captures drag coefficient versus Reynolds number for values of Reynolds number up to 106. The equation proposed by Renauld et al. is valid to Reynolds number up to 100; it was developed based on some dimensionless numbers such X(n), β and b, the drag coefficient in creeping region, C_{Do}, the drag coefficient in the Newton region, $C_{D\infty}$, the surface area of a sphere, Ac, and the cross-sectional area of a sphere, Am. The analysis is built around the mean shear rate deduced from the system's overall rate of energy dissipation. The last equation shown in table 5 is the equation of balance of forces used to obtain the experimental value of the drag coefficient.

For each experimental test, there is a velocity evolution; as the variation between the behaviors of velocity graphs is minimal, the velocity starts null and increases until it reaches a stable value, so it is not necessary to present the graphs for each test. Figure 10 presents the velocity evolution of experimental tests for a 3mm diameter sphere in a Newtonian fluid.

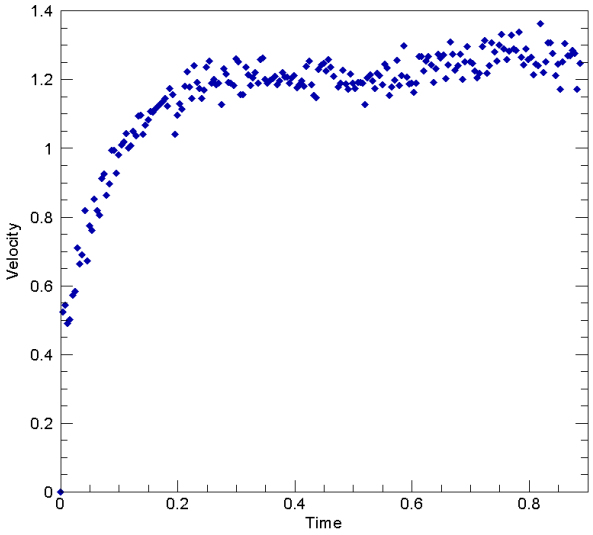

Figure 10. Variation of velocity by the time of the 3 mm diameter particle in fluid N1.

This work also approaches trajectories of the particles during sedimentation. For better analysis, the graphs were plotted with dimensionless, so it is possible to see the trajectory behavior. For the spheres, the work of Horowitz and Williamson (2010) will be used as a reference for evaluating this behavior.

Figure 11 depicts the trajectory of the spheres during the sedimentation in the Newtonian fluid N1, where is possible to observe the spheres with diameter 2 mm and 4.76 m falling straightly. Horowitz's work does not approaches this mass ratio (m*), which is the ratio between the particle density and the fluid density, but comparing the same Reynolds range, it is possible to observe this behavior in tests performed with Re ≥ 1550. The 5mm sphere, on the other hand, falls obliquely. The sphere with a diameter 3 mm differs in its tests. One falls straighter while the other falls obliquely; this can be explained by the release method, as this configuration was the initial test, so the mechanism was not ready, and the release was made with tweezers. It is interesting to note that due high speed of this article, there are many oscillations that can be explained due to low frame rate. Figure 11 shows oblique trajectories for all the cases, and the oblique behavior is more notorious with the increase of the sphere diameter.

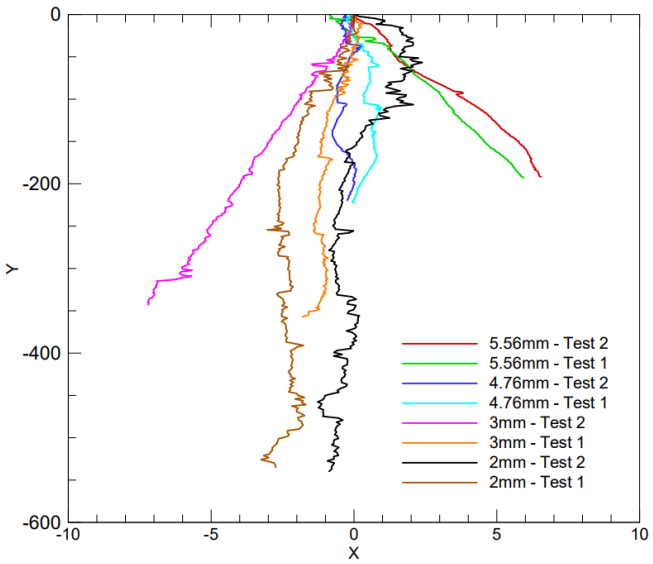

Figure 11. Trajectories of tungsten spheres in the fluid N1.

On the other hand, Fig. 12 shows the settling trajectories of the spherical particles in the fluid N2. The particles with diameter 3.125 mm, 4.762 mm, 6.35 mm falling straightly, while the particles with a diameter of 8 mm and the particles of 10 mm have a sedimentation trajectory that resembles oblique intermittent reaching an oscillatory behavior.

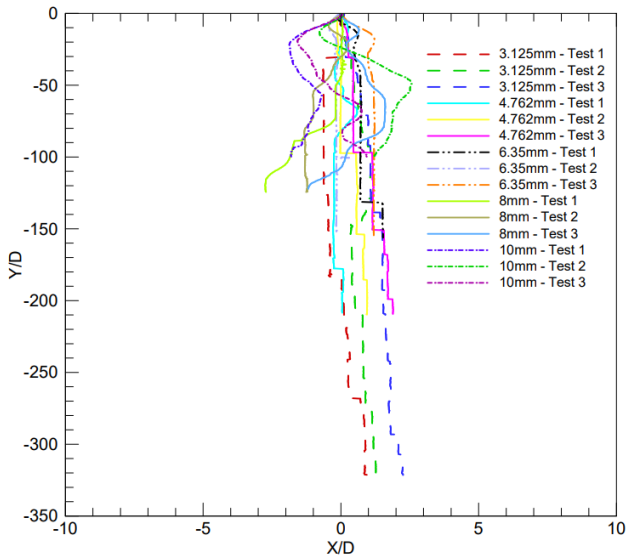

Figure 12. Trajectories of polyacetal spheres in the fluid N2.

In Figure 13 are the tests of spheres in fluid C1, it is possible to see the particles with diameters 6.35 mm, 8 mm, and 10 mm falling obliquely. Due to difficulties in viewing the particle in the experiment, the 6.35mm diameter particle trajectories are shorter. Nevertheless, the trajectory tends to same oblique behavior as the other spheres.

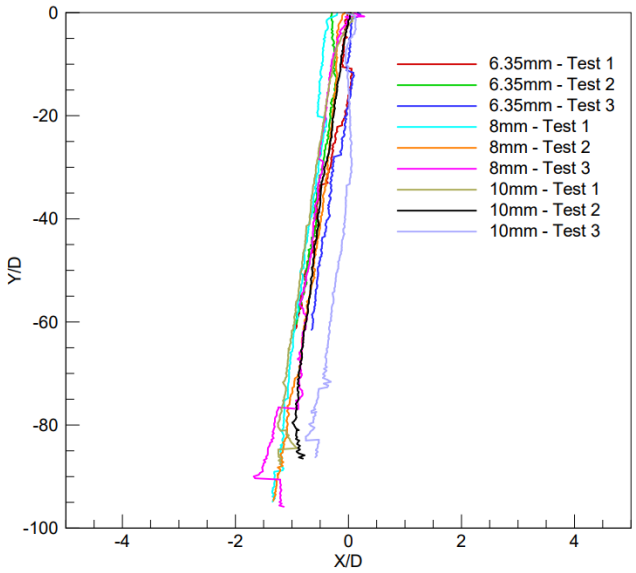

Figure 13. Trajectories of polyacetal spheres in the fluid C1.

3.2 Ellipsoids

Figures 14 shows the average velocities, the average CD, and the average Reynolds as a function of the particle flatness. For the non-spherical cases performed by ellipsoid particles, the velocity, and consequently the Re, comprehends a reduction for the fluid C1, while the drag coefficient increases. This can be explained by an increase in the area in direct contact with the fluid. Interestingly, regardless of how the ellipsoid was released into sedimentation, it rotated so that its largest area was normal to the settling direction.

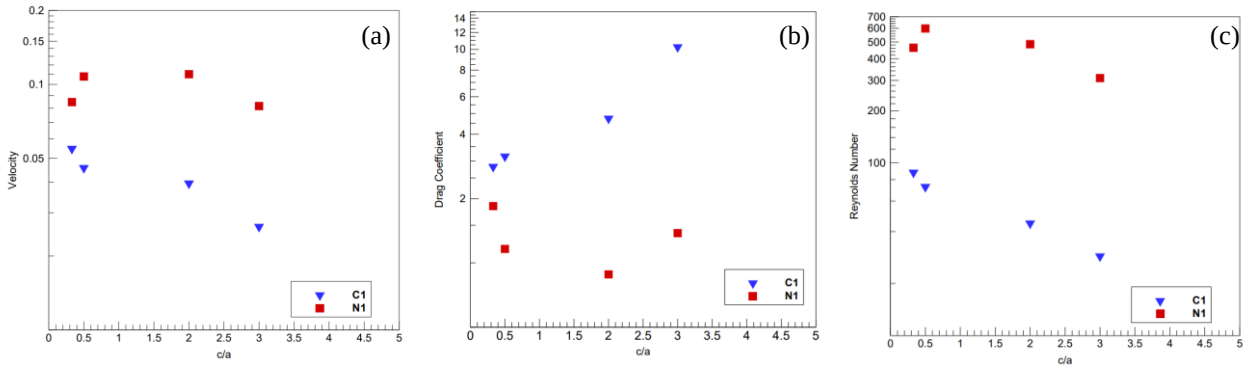

Figure 14. Experimental data of ellipsoids tests. a) Average terminal velocity by the flatness. b) Average C_D by the flatness. c) Average Reynolds by the flatness.

For ellipsoids, the work of Horowitz and Williamson (2010) cannot be used as a reference for evaluating this behavior, however, will be used the same denomination for the behaviors. Figure 15 depicts the trajectory for the ellipsoids in the fluid N1. The axes were made using the equivalent diameter for each particle.

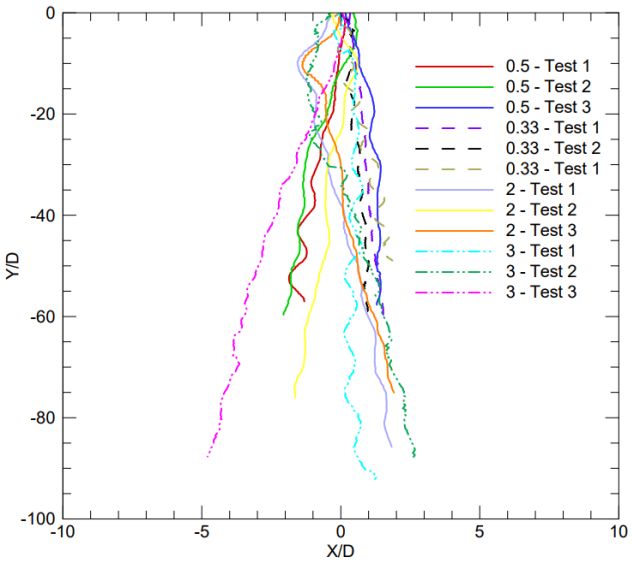

Figure 15. Trajectories of ellipsoids in fluid N1.

For particles with flatness 2 and 3, the behavior can be described as oblique, while the behavior is straightly fall for the other particles. It is interesting to note that the movement that gives the sensation of horizontal oscillation is negligible because it is too small, about 1 time the equivalent diameter of the particle, and it can be explained by particle oscillation, which makes the software used to have this perception of movement.

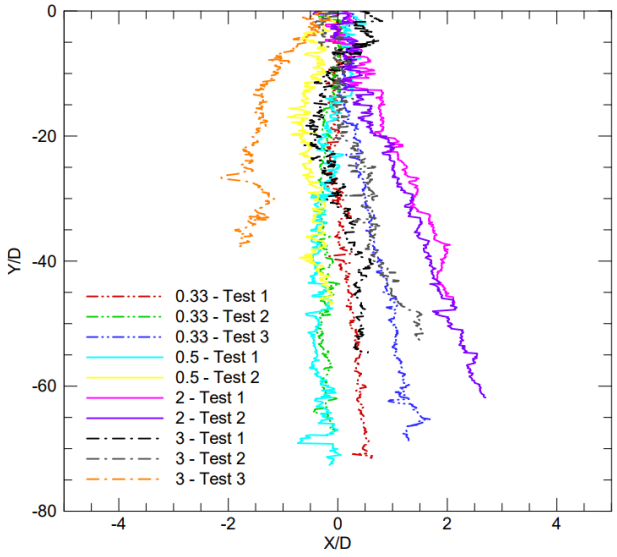

Figure 16. Trajectories of ellipsoids in fluid C1.

In Figure 16, the behavior observed for the particle with flatness 2 can be described as an oblique fall, such as was observed in tests in the N1 fluid. For the particle with 0.33 of flatness, the behavior can be described as a rectilinear movement for tests 1 and 2 once the variation is maximum is 0.5 times the diameter, test 3 presents an oblique behavior. In tests with a particle with flatness 0.5, the behavior straightly falls since the variation stays between -0.5 and 0.5. Test 1 for a particle with flatness 3 presents fall behavior straightly, the tests 2 and 3 presents an oblique behavior. As observed in Figure 14, there are viewing problems due to the oscillation of particles in sedimentation, so small variations can be despised. Besides, the tests realized in this fluid were a poor visualization due to the characteristic opacity of Carbopol®.

In a Newtonian fluid, the trajectory seems to vary between oblique and oscillatory. Furthermore, it is possible to notice from how the ellipsoids move that the flatter particles appear to have a bigger oscillation. It may be due to the larger area normal to flow, as ellipsoids with greater flattening look like a disk, while those with less flattening resemble a grain of rice. For the Power-law fluid, despite the noise caused by the opacity of fluid, the trajectory seems to be more oblique with a kind of transition to oscillatory but without a defined pattern. It seems that the same thing happens in the spheres. The regime is more “disturbed” for the Newtonian and a little more orderly in the Power-law fluid.

4. CONCLUSIONS

The paper presents a study of the body dynamics of particles falling freely through fluids with different rheological characteristics. Velocity, drag coefficient, and trajectory were analyzed using a translucent container tank with an infrared system to release the particles as the experimental setup. Therefore, 12 initial tests were performed with spherical particles varying the Reynolds number and mass ratio m*, then, it is possible to observe the importance of these two parameters to evaluate velocity, drag coefficient, and trajectory by correlations for these parameters, as also the rheological properties of the fluid that plays an essential role in the sedimentation process.

For Newtonian fluids, tests were performed with a Reynolds interval between 50 and 9,000 for spheres and values between 300 and 600 for ellipsoids. The values for drag coefficient founded in lower Reynolds were higher than values in higher Reynolds, and this happened due to the increase in diameter and decrease in settling velocity. For non-Newtonian fluid, the drag coefficient is even higher due to the bigger fluid consistency of a Power-law fluid, even with lower Reynolds numbers, between 20 and 60 for spheres and values between 20 and 90 for ellipsoids.

Finally, we concluded that the rheological properties seem to affect the sedimentation regime of the particles. Further, the fluid with thinning properties and greater consistency reduces the disturbance or the tendency to chaos during sedimentation, the greater resistance can explain this to the movement. Another factor analyzed was the geometric shape, which also influences if the particle is not spherical, it tends to have more disturbed sedimentation than a sphere. This can be because when the spherical particle tends to rotate around its axis, it is only rotational, whereas, for a non-spherical particle, this becomes a little more complicated since to rotate around its axis it needs to move fluid, which generates an extra resistance and causes the vibration observed.

4.1 Limitations and futures steps

Due to the COVID-19 world pandemic, we had logistical issues, and some equipment limitations were not resolved. The realization of all the initial planned tests was compromised. So, it was not possible to perform tests on the viscoplastic fluid as previously planned. Thus, future works will be approached the sedimentation of particles spherical and non-spherical in viscoplastic and thixotropic fluids as the aim of the present experimental project.

5. ACKNOWLEDGEMENTS

The authors would like to thank the Academic Mechanics Department - DAMEC / UTFPR, to the Research Center for Rheology and Non-Newtonian Fluids - CERNN, and the National Agency of Oil, Natural Gas and Biofuels - ANP.

6. REFERENCES

Elgaddafi, R.; Ahmed, R.; George, M.; Growcock, F. Settling behavior of spherical particles in fiber-containing drilling fluids. Journal of Petroleum Science and Engineering. n. 84-85, p. 20-28, 2012.

Eltilib, R. A. E. E.; Kayiem, H. H. A.; Jaafar, A. Investigation on the particle settling velocity in Non-Newtonian fluids. Journal of Applied Sciences. n. 11, 1528-1535, 2011.

Faith, M.A. Data Correlation for Drag Coefficient for Sphere. <www.chem.mtu.edu/~fmorriso/DataCorrelationForSphereDrag2016.pdf.>. Accessed 9 May 2021.

Nunes, J. F.; Ataíde, C. H.; Melo, F. R. G. Velocidade terminal de esferas em líquidos não newtonianos. In: CONGRESSO BRASILEIRO DE ENGENHARIA QUÍMICA EM INICIAÇÃO CIENTIFICA, 5, 2004, Curitiba.

Renaud, M., Mauret, E., & Chhabra, R. P. (2004). Power-law fluid flow over a sphere: Average shear rate and drag coefficient. The Canadian Journal of Chemical Engineering, 82(5), 1066-1070.

Reynolds, P. A; Jones, T. E. R. An Experimental Study of the Settling Velocities of Single Particles in Non-Newtonian Fluids. International Journal of Mineral Processing. n. 25, p. 47-77, 1989.

Song, X; Xu, Z.; Li, G.; Pang, Z.; Zhu, Z. A new model for predicting drag coefficient and settling velocity of spherical and non-spherical particle in Newtonian fluid. Powder Technology. n. 321, p. 242-250, 2017.

Horowitz, M.; Williamson, C.H.K. The effect of Reynolds number on the dynamics and wakes of freely rising and falling spheres. Journal of Fluid Mechanics. N. 651, p 251-294, 2010.

Veldhuis, C. H. J.; Bielsheuvel, A. Na experimental study of the regimes of motion of spheres falling or ascending freely in a Newtonian fluid. Journal of Multiphase Flow. n. 33, p. 1074-1087, 2007.

Xu, Z.; Song X.; Li, G.; Pang, Z.; Zhu, Z. Settling behavior of non-spherical particles in Power-law fluids: Experimental study and model development. Particuology. n.46, p. 30-39. 2019

7. RESPONSIBILITY NOTICE

The authors are the only responsible for the printed material included in this paper.